

Cite as: Woodcock, J.W., Beams, R., Davis, C.S., Chen, N., Stranick, S., Shah, D.U., Vollrath, F., Gilman J.W. *Observation of interfacial damage in a silk-epoxy composite, using hyperspectral and fluorescence lifetime imaging of a simple mechanoresponsive fluorescent probe*. **Advanced Materials Interfaces**, 2017, 1601018. DOI: 10.1002/admi.201601018

Observation of interfacial damage in a silk-epoxy composite, using a simple mechanoresponsive fluorescent probe

Jeremiah W. Woodcock^a, Ryan Beams^a, Chelsea S. Davis^a, Ning Chen^a, Stephan J. Stranick^a, Darshil U. Shah^{b,†}, Fritz Vollrath^b, Jeffrey W. Gilman^{a†}

^aMaterials Measurement Laboratory, National Institute of Standards and Technology, Gaithersburg, Maryland, USA

^bOxford Silk Group, Zoology Department, Oxford University, Oxford, United Kingdom

[†]Correspondence and requests for materials should be addressed to J.W.G at

jeffrey.gilman@nist.gov.

[‡]Present Address: Centre for Natural Material Innovation, Dept. of Architecture, University of Cambridge

* Official contribution of the National Institute of Standards and Technology (NIST); not subject to copyright in the United States. Description of commercial products herein is for information only; it does not imply recommendation or endorsement by NIST.

Keywords: composites, fluorogenic, mechanophore, Rhodamine^{*}, uniaxial deformation, single fiber, silk, epoxy

Polymer based composite materials are ubiquitous in our physical world. Natural examples include wood, crustaceans' exoskeleton, and bone; while man-made examples range from applications in aerospace structures and transportation vehicles, to biomaterials, and sporting goods^[1-4]. In fact, demand for lightweight, energy saving, composites are growing faster than industry's current ability to respond; this mismatch between supply and demand is due not only to the large variety and volume of composites required, but also the unprecedented coupled expectations for performance.

The materials comprising polymer composites are diverse. The reinforcing phase, whose dimensions can range from the nanometer scale to the meter scale, can be mineral, glass, carbon, or biomaterial in origin. The polymer matrices can be equally varied in make-up: they can be protein or polysaccharide, as in natural composites, or fabricated from any of the myriad of commercially available polymers. A unifying characteristic across all of these related classes of materials is the presence of an interface where the components meet. Here, the *interface* is defined as the area of contact between the reinforcement and matrix^[5]. The impact of the interface has been studied and found to be critical in the determination of composite properties^[6-9].

Fiber reinforced polymer composites (FRPC) are an interesting and important class of composites, because they combine the beneficial attributes of the two components: namely, the strength of the fiber and the toughness of the polymer matrix. However, this synchronistic effect is only possible when there is efficient stress transfer across the interface from the matrix into the fiber. The quality of the interface determines the efficiency of stress transfer⁷⁻⁹. The nature of the interface is determined by several factors such as the composition of the two

components, their morphology, physical properties, and the nature of association between them. Interfacial strength is governed by mechanical adhesion, chemical attachment, electrostatic forces and inter diffusion^[10–12]. Several methods exist to interrogate the strength of a FRPC interface, including single fiber fragmentation and microdebonding^[13–15]. These methods are effective for determining interfacial strength, but do not provide a complete understanding of crucial factors, such as the failure mechanisms at the interface, and the chemical and physical properties of the interphase. Without a fundamental understanding of interfacial properties, robust design rules and accurate predictive models necessary to address the growing need for composites cannot be developed. Efforts focused on obtaining fundamental information about the interface include studies of model polymer-composite interfacial interactions using neutron reflectivity, and fluorescence spectroscopy of probe labeled substrates^[8,16]. Other recent work has succeeded in improving our understanding of the interphase in polymer composites using *imaging* techniques, such as atomic force microscopy, Förster resonance energy transfer, infrared microscopy, birefringence, and Raman microscopy^[17–21]. These imaging methods provide direct observation of the quantity, spatial distribution, and heterogeneity of the interphase in the composite. However, additional measurement tools that allow direct measurement of the polymer composite interface in response to *realistic deformation* are needed.

Here, we report direct observation of interfacial damage, using two-photon fluorescence life-time imaging microscopy (TP-FLIM), following uniaxial tensile deformation of a silk fibroin epoxy composite (Figure 1). This was accomplished using a simple two-step process to incorporate a mechanoresponsive fluorescent probe at the interface, combined with the use

of hyperspectral fluorescence imaging and TP-FLIM characterization. The spectral and life-time data confirmed the extent of covalent bonding of the probe at the interface. This measurement platform (multi-modal fluorescence microscopy coupled with mechanoresponsive probes) shows potential as a powerful tool to accelerate the development of process-structure-property relations in composites.

In the design of this measurement platform we considered a range of molecular probes to incorporate at the interface. Molecular probes have been reported which are responsive to water uptake, mechanical and thermal strain, light, or electrical potentials^[16,22–26]. Of particular interest are fluorogenic probes that transition from a dark state to an emitting state, and whose fluorescent properties, such as fluorescence lifetime (FLT), respond to changes in its environment. One such class of molecular probes change their spectral (absorbance and/or emission) properties in response to mechanical strain, and are termed mechanochromic, or mechanoresponsive. A specific example of a responsive probe is the rhodamine spirolactam (RS) derivative shown in Figure 1a. RS was introduced as an ion sensor and later employed as a UV activated fluorophore for super resolution imaging^[27,28]. Recently RS was incorporated into a polyurethane matrix, and showed multiple activation pathways in the form of pH, light, and mechanical strain^[24]. In this work, we explore the use of Rhodamine spirolactam, RS, based dyes, as interfacial damage sensors and chemical probes, combined with the use of hyperspectral fluorescence imaging and TP-FLIM characterization. RS probes are particularly attractive due to their commercial availability, ease of chemical attachment, thermal reversibility, photo stability, and known activation behavior^[29].

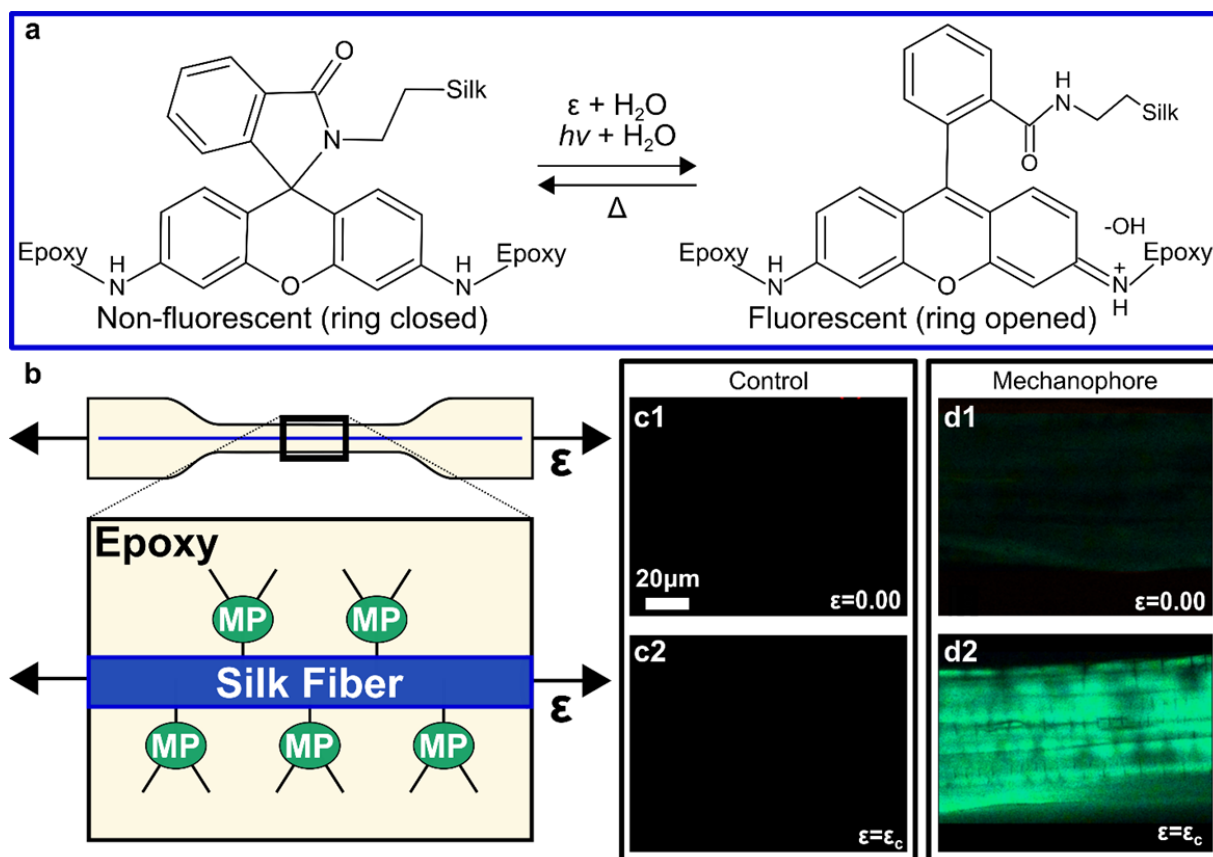


Figure 1: Imaging of stress transfer across a composite interface using mechanically responsive spirolactam (Rhodamine 110, mechanophore). (a) Proposed activation mechanism for the ring opening of the spirolactam through applied energy and in the presence of water. (b) Schematic of a single fiber bundle composite tensile sample with MP covalently attached across the interface between the silk fiber bundle and epoxy matrix. (c1-c2, d1-d2) Two photon fluorescence lifetime microscopy (2P-FLIM) images of single fiber bundle silk epoxy composites before (c1, d1) and after (c2, d2) strain. (c1-c2) Fluorescence images of the control (Rhodamine-B functionalized silk fiber bundle in epoxy with non- reactive amine groups, CT), shows no activation within experimental parameters. (d1-d2) Significant activation of MP is observed in response to uniaxial mechanical strain.

Rhodamine 110 serves as a mechanophore (MP) and contains three reactive sites (SI Scheme1), allowing it to be chemically bound across the interface of the silk-epoxy composite (Figure 1b). Introduction of this fluorophore at the interface is achieved through a straightforward attachment of the MP to the silk followed by covalent reaction of the probe with the epoxy matrix. Rhodamine B is employed as a control (CT) because it has only one

reactive site, allowing attachment to the silk fiber, but preventing subsequent covalent reactions with the epoxy matrix. The process of mechanical activation is thermally reversible at moderate (100 °C) temperatures, where the strained (closed, non-fluorescent) spirolactam structure is recovered through restoration of the aromaticity of the peripheral phenyl rings. The necessity of advantageous water for activation of the rhodamine spirolactam system, in order to maintain the conjugated fluorescent center (xanthene) was observed as well. This process is not well understood and requires further study. In addition, using spectral and lifetime imaging, the extent of reaction of the epoxy with the aromatic amines of the fluorophore was qualitatively observed, revealing that the extent of cure can be monitored across the interface using shifts in the fluorescence wavelength of emission in conjunction with fluorescence lifetime.

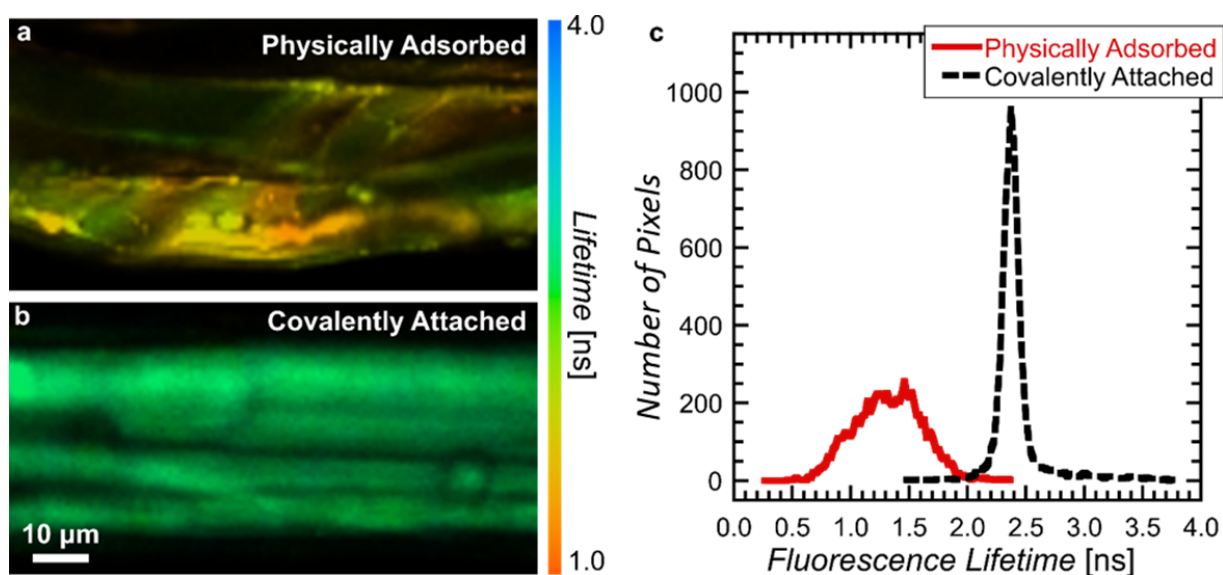


Figure 2: 2P-FLIM analysis of physically and covalently labeled silk fiber bundle lifetime distributions. FLT image of (a) physically adsorbed and (b) covalently attached MP on silk fiber bundle. The color scale to the right of the images indicates FLT values and applies to both

images. (c) Comparison of average FLT distributions for physically adsorbed and covalently. The covalently attached dye shows a narrower FLT distribution and a longer average lifetime.

To position the MP at the interface, a simple approach was developed that takes advantage of the pendant group functionality of the silk protein. Silk fibroin has a complex structure with varying crystalline and amorphous regions. Previous studies have shown that the crystalline region is comprised of β sheets with internalized polar moieties, with alanine and glycine dominating the protein sequence^[30,31]. The amorphous regions, which can make up to 45 mass fraction of the protein structure, have an assortment of amino acids with the primary amine of lysine being the most probable reaction site^[32]. Fibroin of *Bombyx Mori* has been shown to contain 0.2 mole % lysine indicating a maximum theoretical functionalization^[33]. This small level of alteration of the protein was viewed as ideal for fluorescence measurements while minimizing alteration of interfacial interactions. Using TP-FLIM, covalent attachment of the probe molecule was observed after base catalyzed reaction, between the silk and the carboxylic acid group of the MP; most likely through amide bond formation followed by ring closure to form the spirolactam (Sl. Scheme 1). Figure 2 shows fluorescence life-time (FLT) maps of two silk fibers along with the corresponding FLT distributions. The physically absorbed MP-silk fiber sample (figure 2a) shows a much shorter fluorescent lifetime, as well as a broader distribution (figure 2c) than the fiber that was covalently functionalized with MP. It is well known that a loss of degrees of freedom in a fluorescent molecule results in an increase of fluorescence lifetime^[34,35]. This can be spawned through fewer non-radiative pathways available for the relaxation process of the fluorescent center. Chemical environment effects and suppression of degrees of freedom leading to an increase in lifetime have been observed in

the biological and polymer communities through cell, DNA, protein, and polymer confinement studies. The common result being shorter lifetimes can be attributed to fluorescence quenching, non-radiative energy loss through dimerization, and interactions with different chemical environments^[36–38]. The fiber with the MP covalently attached (figure 2b) shows a narrow FLT distribution (figure 2c), as well as a significantly longer average FLT. This is the difference typically observed between a physically absorbed dye and a covalently bonded dye^{[39][40,41]}. Attachment of the MP to the silk fiber by the spirolactam ring leaves the aromatic amine groups available for crosslinking with the matrix monomer.

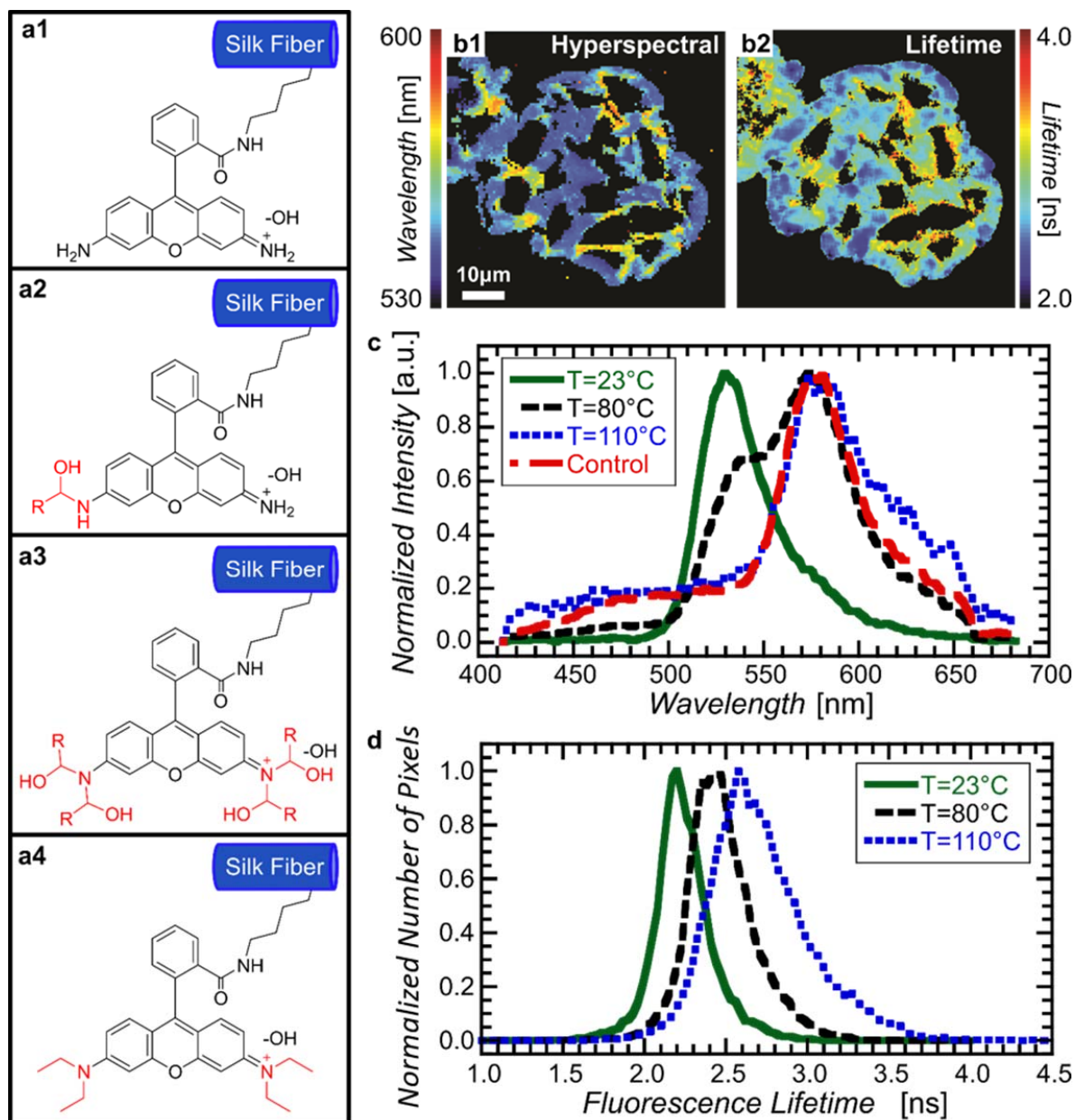


Figure 3: Extent of reaction of the primary aromatic amines of MP functionalized silk fiber with the epoxy matrix as a function of cure temperature. (a1) Structure of MP, (a2, a3) two possible reaction products and (a4) Rhodamine-B (control, CT). Each amine in MP is capable of forming two bonds with the epoxide monomer. (b) Cross sections of MP functionalized silk fiber-epoxy cured at 80 °C. As additional alkyl substituents are reacted with the MP, the fluorescence emission shifts to longer wavelengths (b1, hyperspectral image) and longer FLTs (b2, 2P-FLIM) as shown by the false color maps. (c) Fluorescence emission of labeled fiber-epoxy cross sections with increasing matrix curing temperatures. The fluorescence emissions show an increase in emission wavelength with increasing curing temperatures with a bimodal spectrum observable at 80 °C. (d) FLT distributions of labeled silk fiber bundle cross sections at different cure temperatures. As the cure temperature increases, the

average lifetime distribution shifts to longer lifetimes indicating a decrease in non-radiative processes from additional bonds and reduced mobility. For microscope settings and resolution information see S.I.

Following attachment of the MP to the silk, further reaction of the probe with the epoxy was investigated. Single fiber-bundle silk epoxy composites were prepared at different curing temperatures to optimize the extent of MP attachment to the epoxy matrix. Figure 3 (a1-a3) shows the attachment schemes of the silk-MPs with the epoxy monomer. Rhodamine B was used as a control (Figure 3 a4), since the diethyl-functionalized amines approximate a fully reacted version of the MP, yet lacks the reactivity of the primary aromatic amines of the MP. This prevents covalent attachment of the CT-dye to the epoxy.

The reaction of the silk-MP with the epoxy matrix is temperature dependent. The proposed reaction products from reaction of the silk-MP (Figure 3 a1) with the epoxy are shown in Figure 3 a2 and Figure 3 a3. Hyperspectral imaging, where a spectrum is acquired in each pixel, was used to study chemical changes of the silk-MP at the interface after reaction with the epoxy matrix. The emission spectra of the region of interest displayed in Figure 3 b1 and plotted in Figure 3 c, show evidence of the reaction of the MP with the epoxy matrix. This increase of the MP maximum emission wavelength (λ_{em}) from 525 nm to 580 nm with increasing matrix curing temperatures is expected, since increasing electron donating characteristics of a fluorescent molecule typically produces a shift to longer wavelengths (red shift)^[42–44]. It is anticipated that the 23°C sample only undergoes cure between the curing agent and the epoxy, no MP cure occurs due to the lower reactivity of the aromatic amines. The λ_{em} for the samples cured at 80 °C and 110 °C are similar to the λ_{em} of the CT (Figure 3 a4). When the composite was cured at 80 °C, the λ_{em} showed a bimodal emission spectrum at about 530 nm and 580 nm as seen in Figure 3c. The 80 °C hyperspectral data show a transition between the unreacted (or

partially reacted) MP and fully reacted MP. Figure 3 b1 shows the cross sectional view of the sample cured at 80 °C using hyperspectral imaging. It can be observed that the reaction is quite heterogeneous, with dye molecules located on the outer surfaces of the fibers showing the largest extent of reaction as seen by the yellow, orange and red areas. By monitoring λ_{em} , critical information about the local chemical environment at a composite interface can be obtained. Such techniques also show promise to be utilized for monitoring the degree of interfacial curing.^[45–47]

Confirmation of the above conclusions can be drawn from the TP-FLIM image of the 80 °C cured sample, shown in Figure 3 b2. The spatial distribution of lifetimes in the image is heterogeneous with longer lifetime regions localized near the fiber surfaces. Qualitatively, this TP-FLIM image spatially correlates with the hyperspectral image in Figure 3 b1. That is, regions with longer lifetime qualitatively also have longer λ_{em} . The TP-FLIM images for the T = 23 °C and T = 110 °C cross sections are provided in SI Figure 7. SI Figure 8 shows a plot of Fluorescence lifetime versus wavelength. The scatter plot shows an 85% correlation between increase in lifetime and increase in wavelength value for the sample cured at 80 °C.

Immobilization of a fluorophore results in a longer FLT^[48,49]. The lifetime distributions, taken from the TP-FLIM cross section images, of the three samples cured at increasing temperatures are shown in Figure 3d. These distributions shift to longer lifetimes with increasing cure temperatures, indicating a possible loss of degrees of freedom for the fluorophore as a result of epoxy reaction with the MP. The lifetime distributions for the 110 °C sample is similar to that for the silk-CT (SI Figure 2c). The greater degree of reaction restricts the available conformations, or relaxation pathways, and produces a longer lifetime. With

covalent attachment at the interface, the MP is positioned to report on stress transfer across the interface from the matrix to the fiber upon uniaxial tensile deformation.

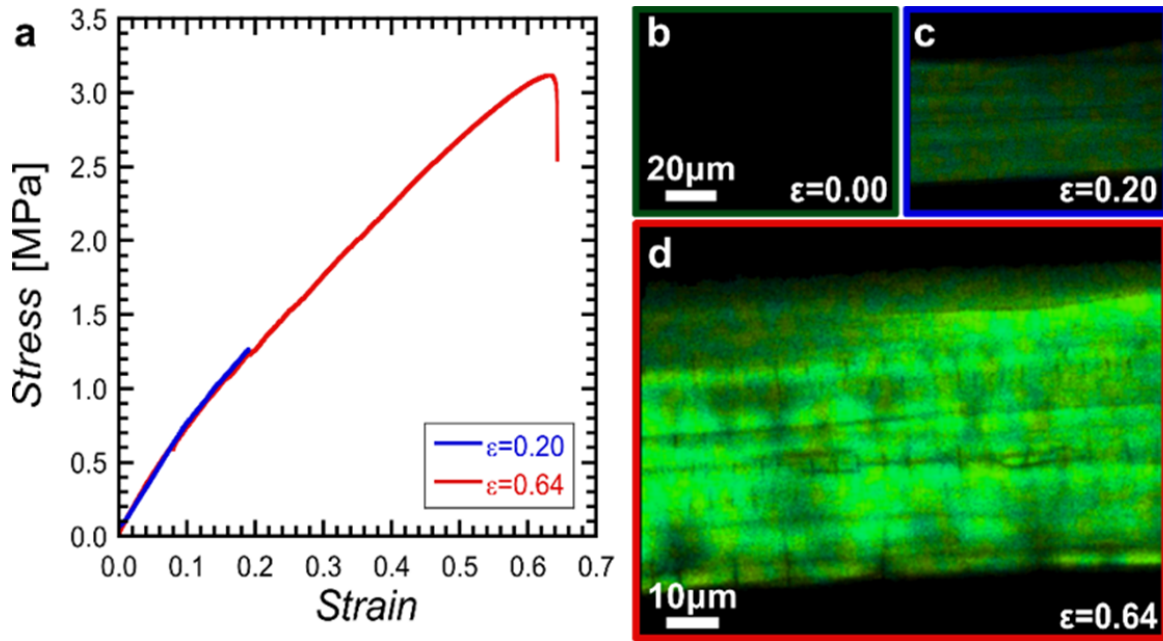


Figure 4: Activation of MP at the interface of a single fiber bundle silk epoxy by mechanical deformation. (a) Uniaxial tensile response of single fiber bundle composites after the application of moderate strain ($\epsilon = 0.20$) and critical strain ($\epsilon = 0.64$). (b-d) Corresponding TP-FLIM images of fiber composites. (b) Prior to deformation, minimal fluorescence is observed. (c) At $\epsilon = 0.20$, a uniform, low intensity fluorescence is observed with minimal visible damage to the fiber surface. (d) At $\epsilon = 0.64$, the sample fractures, the fluorescence intensity is heterogeneous but overall brighter than at moderate strain, and numerous microcracks can be seen on the surface of the fiber bundle.

A fiber composite tensile specimen with a dog bone testing geometry was fabricated by embedding a MP-functionalized silk fiber bundle in a DGEBA-based rubbery epoxy matrix ($T_g = -23\text{ }^{\circ}\text{C}$). The composite was cured at $110\text{ }^{\circ}\text{C}$ for 19 h. The composite was conditioned at 50 % relative humidity for 24 h prior to mechanical testing to ensure the presence of water at the interface to stabilize the activated, ring-opened state of the RS probe. Figure 4 shows the activation of the MP attached across the interface in response to mechanical strain (ϵ). Prior to the application of uniaxial tensile deformation, very little background fluorescence is visible

(Figure 4b). After moderate strain ($\epsilon = 0.20$) is applied, fluorescent activation of the MP is observed, indicating conjugation across the xanthene ring has occurred through ring opening of the spirolactam^[50,51]. Whether this activation arises solely through direct stress transfer along covalent bonds, or if a frictional shear component at the interface contributes to the fluorescence is unclear. The main contribution is expected to be stress transfer through chemical bonds. Control composite samples without dye functionality were tested along with MP containing fibers (SI Figure 6) with similar results indicating minimal impact on physical properties from the dye's presence at the interface. Further and perhaps more convincingly, the CT-functionalized silk-epoxy samples, which lacked covalent attachment of the RS with the epoxy, but would experience interfacial shear forces, showed little to no activation under the same tensile strain conditions (Figure 1c and SI Figure 5A-B).

After critical failure, the fluorescence of the MP-functionalized silk composite is more intense and more heterogeneous, with local areas of higher or lower extents of activation, indicating non-uniform interfacial stresses. These local intensity differences seem to indicate areas of stronger and weaker interfacial strength, highlighting especially strong regions of interfacial bonding where interfacial stress transfer has been localized and a larger number of MP molecules have been sufficiently strained to activate. It should also be mentioned here that the dark regions could also arise from actual damage to the MP if a high enough force is reached to break covalent bonds in the RS probe. Thin dark lines, perpendicular to the fiber axis are thought to be micro-fractures or cracks on the surface of the outermost silk fibers. The origin and structural implications of these cracks will be addressed in future work.

Installation of RS at a composite interface is a powerful, yet simple system for probing stress transfer and damage on a molecular length scale, when combined with hyperspectral and TP-FLIM imaging techniques. The advantages of this system include the commercial availability of the MP precursor, Rhodamine 110, and the simple one-pot fiber functionalization, which simultaneously attaches the dye to the fiber by amidation, and forms the (dark, ring-closed) spirolactam by base-catalyzed cyclization. The attachment of the MP at the interface to the matrix is easily monitored through shifts in λ_{em} or the lifetime. Interfacial MPs have potential as a tool for both fundamental studies of composite interfacial damage (whether through cyclic loading, environmental effects, or a host of mechanical deformations) as well as industrial use as a structural health-monitoring tool when coupled to an embedded fiber sensor for composite structures. More in depth evaluation of the relationship between the fluorescence parameters, such as intensity, lifetime, and dye orientation, and interfacial properties as a function of deformation are underway. The spectral shifts observed with cure temperature are also being investigated as a potential avenue for monitoring interfacial reaction kinetics. Finally, the discovery of the necessity of water for activation to occur provides the opportunity to monitor hydration of the interface.

Experimental:*

Materials: Rhodamine 110 (MP), Rhodamine B (CT), sodium carbonate, ethanol, and the diglycidyl ether of bisphenol A (DGEBA) were purchased from Sigma-Aldrich and used as received. Jeffamine D230 and Jeffamine ED600 polyetheramines were obtained from Huntsman and used as received. Silk fiber of *Bombyx mori* silk moth larvae, degummed via alkaline water treatment was obtained from Oxford University and used as received.

Covalent attachment of MP to silk: Silk fibroin fibers from *Bombyx mori* (16 mg) were placed into a 250 mL round bottom flask with absolute ethanol (100 mL), Rhodamine 110 (5.0 mg, 0.014 mmol) and sodium carbonate (5.0 mg, 0.047 mmol). The reaction mixture was refluxed for 17 h. The silk was purified by sonication in 0.01 mol/L HCl for 10 min followed by similar sonication in deionized water three times. The silk was then extracted using ethanol via Soxhlet extractor for 48 h. Rhodamine 110 functionalized silk was obtained as an off-white slightly orange fiber with a fluorescence maximum emission at 525 nm using 800 nm two-photon excitation.

Covalent attachment of CT to silk: Silk fibroin fiber bundles from *Bombyx mori* (17 mg) was placed in a 250 mL round bottom flask along with Rhodamine B (8.0 mg, 0.016 mmol), sodium carbonate (5.0 mg, 0.047 mmol), and absolute ethanol (100 mL). The solution was then refluxed for 17 h. The silk was purified by sonication in 0.01 mol/L HCl (10 min) followed by deionized water three times (10 min each). The silk was then extracted using ethanol via Soxhlet for 48 h. Rhodamine B functionalized silk was obtained as a slightly pink fiber with a fluorescence emission of 580 nm using a 800 nm two photon excitation wavelength.

Physical adsorption of MP to silk: Silk fibroin fiber was placed in a 250 mL round bottom flask with Rhodamine 110 (5.2 mg, 0.014 mmol), sodium carbonate (5.4 mg, 0.05 mmol), and absolute ethanol (100 mL). The silk was soaked for 17 h then rinsed with ethanol three times to remove the large excess of dye and allowed to air dry. To keep the experimental conditions as representative as possible, the reaction control (physically absorbed) was immersed in a similar reaction solution to the covalent reaction mixture, but was not heated to the temperature required for base catalyzed reaction.

Preparation of single fiber silk-epoxy composite: A single silk fiber bundle was lightly stretched across the cavity of a 400 μm deep silicone dog bone mold. Small glass spacers ($t \approx 180 \mu\text{m}$) were used to position the silk in the center of the cavity. Jeffamine ED600 and diglycidyl ether bisphenol-A (DGEBA) were mixed in a high shear mixer (FlackTek, Inc., SpeedMixer DAC 150 SP) at 365 rad/s for 5 min. The epoxy mixture was then degassed at the corresponding cure temperature in a vacuum oven (13 Pa) for 10 min. The liquid epoxy mixture was then poured into the silk-containing cavity with care being taken to avoid the introduction of air bubbles. The composites were cured in an oven at 80 °C, or 110 °C for 19 h, or cured at room temperature (23 °C) for 48 h. The single fiber composites were then submerged in water overnight to provide a readily available water for activation of RS.

Tensile deformation of silk fiber composites: Uniaxial tensile deformation was applied to single fiber composite specimens using a servo-controlled mechanical testing frame (AdMet Micro 4000). The sample cross section was 2 mm by 1 mm and the fiber bundle diameter at the center of the cross section was approximately 50 μm . A rubbery epoxy (JA ED600, $T_g = -23 \text{ }^\circ\text{C}$) was used to access relatively high strains before ultimate specimen failure. Samples were strained to a finite specified strain (e.g. 0.20, 0.64) at a constant displacement rate of 1 mm/s. The strain was then removed by returning the grips to their initial position at the same rate. Fluorescence imaging was then performed, *ex situ*, on the strained and unloaded samples.

References

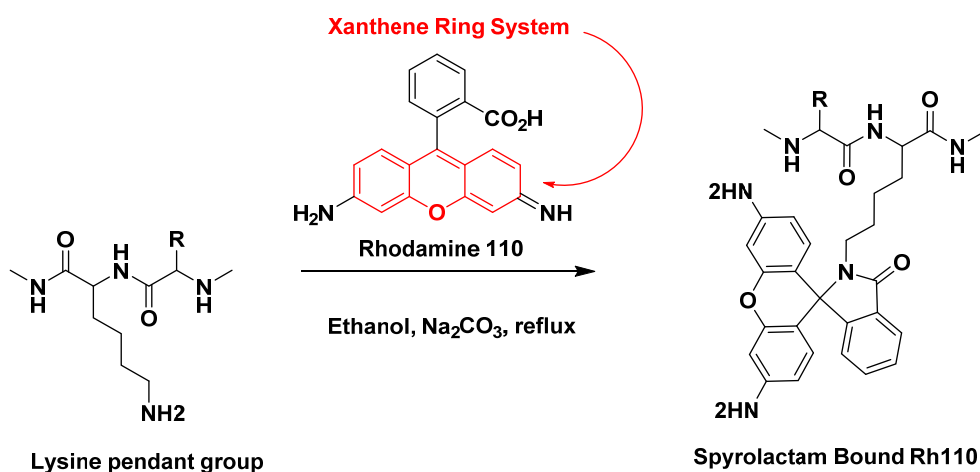
- [1] D. Raabe, C. Sachs, P. Romano, *Acta Mater.* **2005**, 53, 4281.
- [2] M. M. Shenoy, L. V. Smith, J. T. Axtell, *Compos. Struct.* **2001**, 52, 397.
- [3] S. Ramakrishna, J. Mayer, E. Wintermantel, K. W. Leong, *Compos. Sci. Technol.* **2001**, 61, 1189.
- [4] F. Ahmad, H. S. Choi, M. K. Park, *Macromol. Mater. Eng.* **2015**, 300, 10.
- [5] Louis H. Sharpe, *J. Adhes.* **1972**, 4, 51.
- [6] S. L. Gao, E. Mäder, *Compos. - Part A Appl. Sci. Manuf.* **2002**, 33, 559.
- [7] C. Antonelli, B. Serrano, J. Baselga, R. Ozisik, J. Carlos, *Eur. Polym. J.* **2015**, 62, 31.
- [8] J. L. Lenhart, J. H. van Zanten, J. P. Dunkers, R. S. Parnas, *Macromolecules* **2001**, 34, 2225.
- [9] S. a. Eastman, S. Kim, K. a. Page, B. W. Rowe, S. Kang, C. L. Soles, K. G. Yager, *Macromolecules* **2012**, 45, 7920.
- [10] S. Keszei, S. Matkó, G. Bertalan, P. Anna, G. Marosi, A. Tóth, *Eur. Polym. J.* **2005**, 41, 697.
- [11] S. Kang, S. Il Hong, C. R. Choe, M. Park, S. Rim, J. Kim, *Polymer (Guildf)*. **2001**, 42, 879.
- [12] a Kenyon, *J. Colloid Interface Sci.* **1968**, 27, 761.
- [13] C. a. Fuentes, G. Brughmans, L. Q. N. Tran, C. Dupont-Gillain, I. Verpoest, a. W. Van Vuure, *Compos. Sci. Technol.* **2015**, 109, 40.
- [14] R. Bhargava, S.-Q. Wang, J. L. Koenig, *Appl. Spectrosc.* **1998**, 52, 323.
- [15] C. Tascioglu, B. Goodell, R. Lopez-Anido, *Compos. Sci. Technol.* **2003**, 63, 979.
- [16] D. a Davis, A. Hamilton, J. Yang, L. D. Cremer, D. Van Gough, S. L. Potisek, M. T. Ong, P. V Braun, T. J. Martínez, S. R. White, J. S. Moore, N. R. Sottos, *Nature* **2009**, 459, 68.
- [17] P. Schmidt, J. Kolarik, F. Lesnicky, J. Dybal, J. M. Lagaron, J. . Pastor, *Polymer (Guildf)*. **2000**, 41, 4267.
- [18] M. F. Weber, *Science (80-.)*. **2000**, 287, 2451.
- [19] J. Torre, M. Cortázar, M. A. Gómez, C. Marco, G. Ellis, C. Riekel, P. Dumas, *Macromolecules* **2006**, 39, 5564.
- [20] M. Zammarano, P. H. Maupin, L. P. Sung, J. W. Gilman, E. D. McCarthy, Y. S. Kim, D. M.

- Fox, *ACS Nano* **2011**, 5, 3391.
- [21] X. Cheng, K. W. Putz, C. D. Wood, L. C. Brinson, *Macromol. Rapid Commun.* **2015**, 36, 391.
 - [22] Y. Ren, W. H. Kan, V. Thangadurai, T. Baumgartner, *Angew. Chem. Int. Ed. Engl.* **2012**, 51, 3964.
 - [23] Q. Huang, Y. Zhou, Q. Zhang, E. Wang, Y. Min, H. Qiao, J. Zhang, T. Ma, *Sensors Actuators B Chem.* **2015**, 208, 22.
 - [24] Z. Wang, Z. Ma, Y. Wang, Z. Xu, Y. Luo, Y. Wei, X. Jia, *Adv. Mater.* **2015**, 27, 6469.
 - [25] C. R. Hickenboth, J. S. Moore, S. R. White, N. R. Sottos, J. Baudry, S. R. Wilson, *Nature* **2007**, 446, 423.
 - [26] S. M. Oja, J. P. Guerrette, M. R. David, B. Zhang, *Anal. Chem.* **2014**, 86, 6040.
 - [27] H. N. Kim, M. H. Lee, H. J. Kim, J. S. Kim, J. Yoon, *Chem. Soc. Rev.* **2008**, 37, 1465.
 - [28] A. J. Berro, A. J. Berglund, P. T. Carmichael, J. S. Kim, J. A. Liddle, *ACS Nano* **2012**, 6, 9496.
 - [29] L. Möckl, D. C. Lamb, C. Bräuchle, *Angew. Chemie Int. Ed.* **2014**, 53, 13972.
 - [30] J. O. Warwicker, *Acta Crystallogr.* **1954**, 7, 565.
 - [31] K. Okushita, A. Asano, M. P. Williamson, T. Asakura, *Macromolecules* **2014**, 47, 4308.
 - [32] C. Z. Zhou, F. Confalonieri, M. Jacquet, R. Perasso, Z. G. Li, J. Janin, *Proteins* **2001**, 44, 119.
 - [33] A. R. Murphy, D. L. Kaplan, *J. Mater. Chem.* **2009**, 19, 6443.
 - [34] O. Krichevsky, G. BOnnet, *Reports Prog. Phys.* **2002**, 65, 251.
 - [35] L. A. Munishkina, A. L. Fink, *Biochim. Biophys. Acta - Biomembr.* **2007**, 1768, 1862.
 - [36] M. Y. Berezin, S. Achilefu, *Chem. Rev.* **2010**, 110, 2641.
 - [37] J. R. Alcala, E. Gratton, F. G. Prendergast, *Biophys. J.* **1987**, 51, 597.
 - [38] M. K. Mundra, C. J. Ellison, P. Rittigstein, J. M. Torkelson, *Eur. Phys. J. Spec. Top.* **2007**, 141, 143.
 - [39] S. Vajda, V. Fidler, K. Prochazka, **1991**, 2054.
 - [40] C.-C. Chiu, W.-C. Chen, P.-Y. Cheng, *J. Photochem. Photobiol. A Chem.* **2015**, 310, 26.
 - [41] D. W. Phillion, D. J. Kuizenga, a. E. Siegman, *Appl. Phys. Lett.* **1975**, 27, 85.

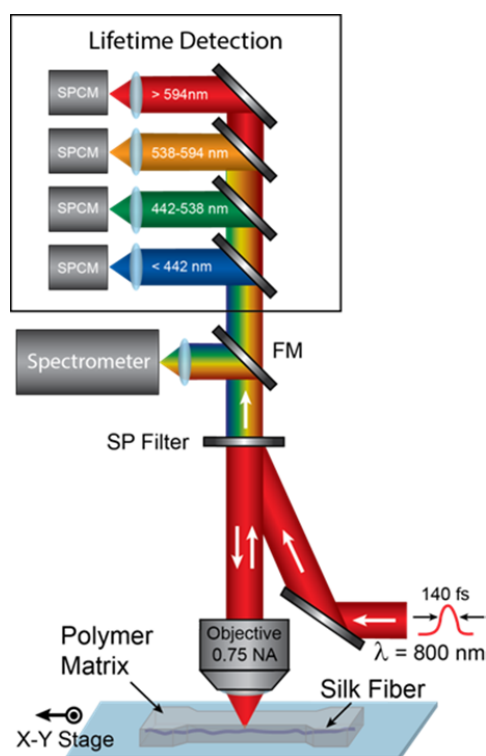
- [42] W. M. F. Fabian, K. S. Niederreiter, G. Uray, W. Stadlbauer, *J. Mol. Struct.* **1999**, 477, 209.
- [43] C. F. A. Gomez-Duran, R. Hu, G. Feng, T. Li, F. Bu, M. Arseneault, B. Liu, E. Peña-Cabrera, B. Z. Tang, *ACS Appl. Mater. Interfaces* **2015**, 150707103126001.
- [44] G. Jones, W. R. Jackson, A. M. Halpern, *Chem. Phys. Lett.* **1980**, 72, 391.
- [45] N. Sbirrazzuoli, S. Vyazovkin, *Thermochim. Acta* **2002**, 388, 289.
- [46] J. González-Benito, *J. Colloid Interface Sci.* **2003**, 267, 326.
- [47] M. Q. Zhang, M. Z. Rong, S. L. Yu, B. Wetzels, K. Friedrich, *Wear* **2002**, 253, 1086.
- [48] M. Y. Berezin, S. Achilefu, *Chem. Rev.* **2010**, 110, 2641.
- [49] J. R. Lakowicz, H. Szmajda, K. Nowaczyk, M. L. Johnson, *Proc. Natl. Acad. Sci. U. S. A.* **1992**, 89, 1271.
- [50] H. Zheng, G. Q. Shang, S. Y. Yang, X. Gao, J. G. Xu, *Org. Lett.* **2008**, 10, 2357.
- [51] J. Huang, Y. Xu, X. Qian, *J. Org. Chem.* **2009**, 74, 5039.

Supplemental Information

SI-1 Attachment of rhodamine 110 to silk fibroin and formation of the RS bond



SI. Scheme 1: Base catalyzed formation of amide bond between silk pendant amine groups and the carboxylic acid of Rhodamine 110 with the most likely reaction site being lysine moieties. Formation of the amide bond is followed by cyclization while heating in the presence of base to give the spirolactam. This establishes aromaticity within the peripheral rings of the xanthene system.



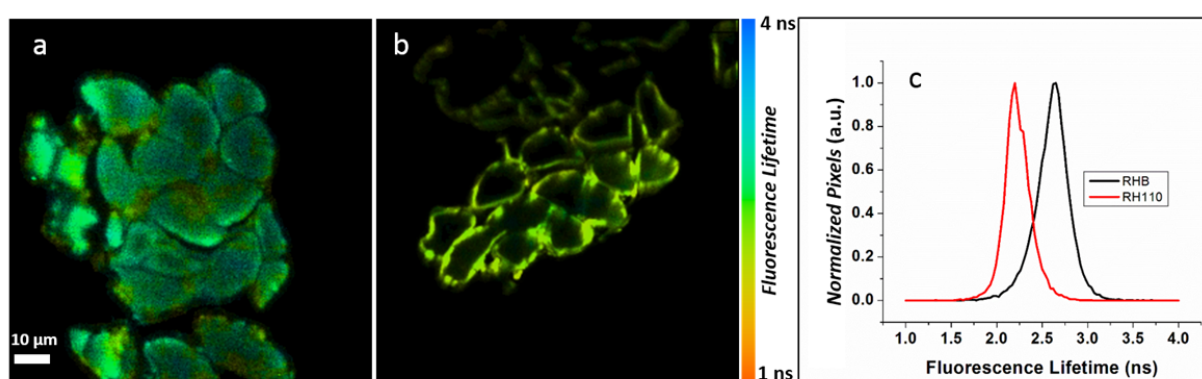
SI Figure 1: Sketch of the optical setup. A Ti:Sapphire operating at 800 nm was used to excite the sample through a 0.75 NA objective. The sample was raster scanned through the laser focus using an X-Y piezo stage and the resulting fluorescence was collected through the same objective and sent to a spectrometer or to lifetime detectors. The wavelength detection range for each single photon counting module (SPCM) is indicated in the illustration. SP = short pass filter. FM = flip mirror

S.I. 1. Optical Measurements

The optical measurements were performed using a NIST-built two-photon fluorescence microscope utilizing a Ti:Sapphire with a pulse width of 140 fs operating at 800 nm. The sample was excited through an air objective with a numerical aperture (NA) of 0.75 and magnification of 40X with a resolution of 400 nm in xy and 800 nm in z. The sample was raster scanned through the laser focus using an X-Y piezo scan stage to build up images. The resulting fluorescence was collected using the same objective and sent to either a spectrometer and

charge coupled device (CCD) or to a series of single photon counting modules (SPCM) for fluorescence lifetime measurements. For lifetime measurements, the fluorescence was spectrally separated using dichroic beam splitters into four channels, as indicated in Figure S1. This allowed for fluorescence lifetime images over four spectral windows to be acquired simultaneously.

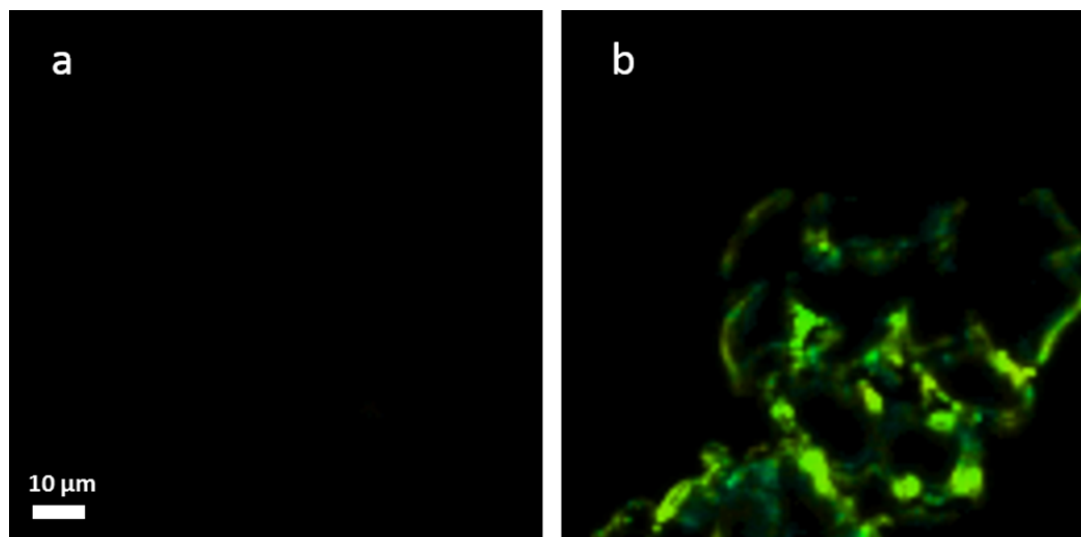
S.I.-2 Extent of Dye Functionalization of Control versus Mechanophore



S.I. Figure 2 Cross sections show the extent of labeling of silk fibroin fiber bundles. The control CT (a) showed almost complete penetration of the fiber bundles, while MP cured at 23 °C (b) remained on the periphery. This shows a larger affinity for the CT to the silk fibroin permitting more extensive labeling under similar reaction conditions. The lifetime distributions (c) show the CT to have a longer lifetime than the 23 °C MP which is the result of less rotational freedom originating from the ethyl groups on the CT xanthene system.

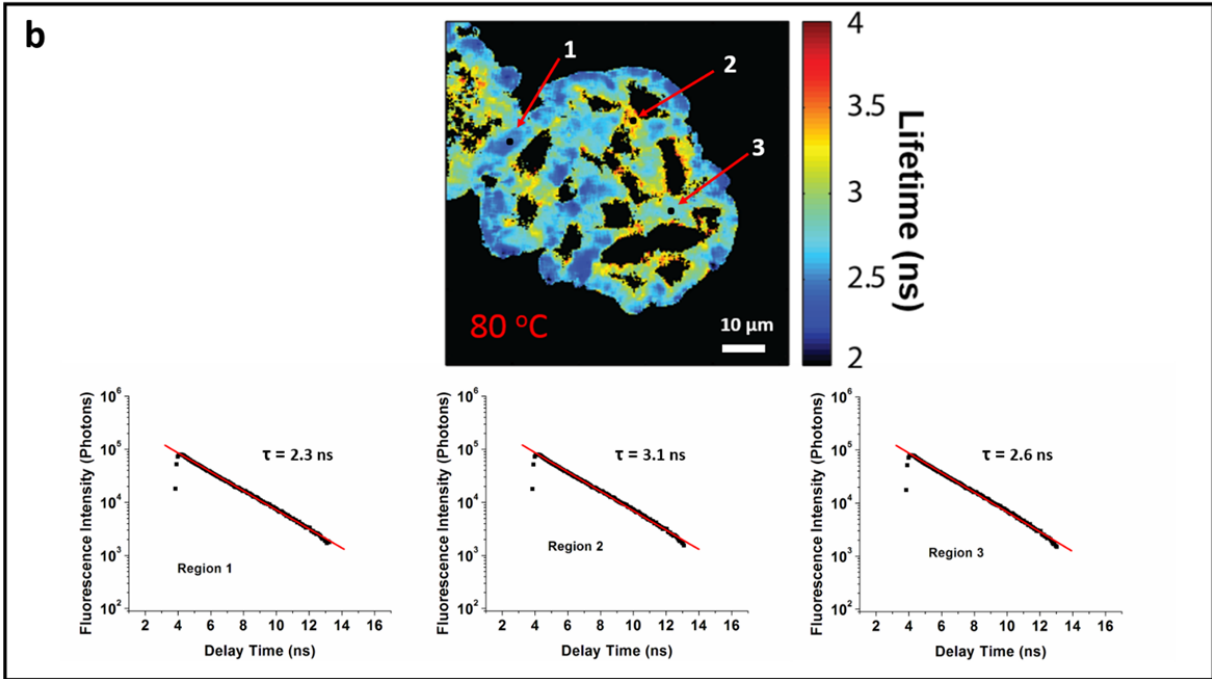
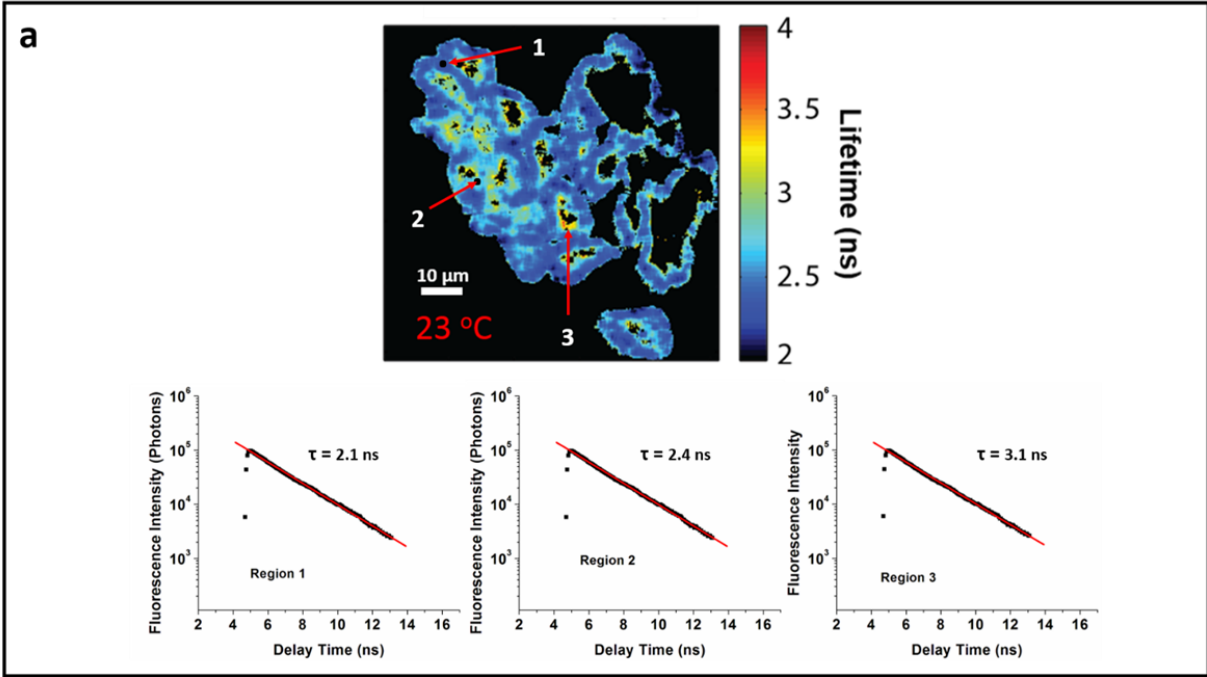
Fiber bundles were functionalized with CT and MP under similar reaction conditions. The CT diffused deeper into individual silk fibroin fibers (S.I. Figure 2a-b). With CT being more hydrophobic, the CT had a higher affinity for the silk. The fluorescence lifetime distributions were also found to be significantly different (S.I. Figure 2c). The CT showed a significantly longer lifetime distribution than MP. This is believed to be the result of steric hindrance provided by the ethyl groups on the amines of the xanthene ring of CT hindering the dye's degrees of

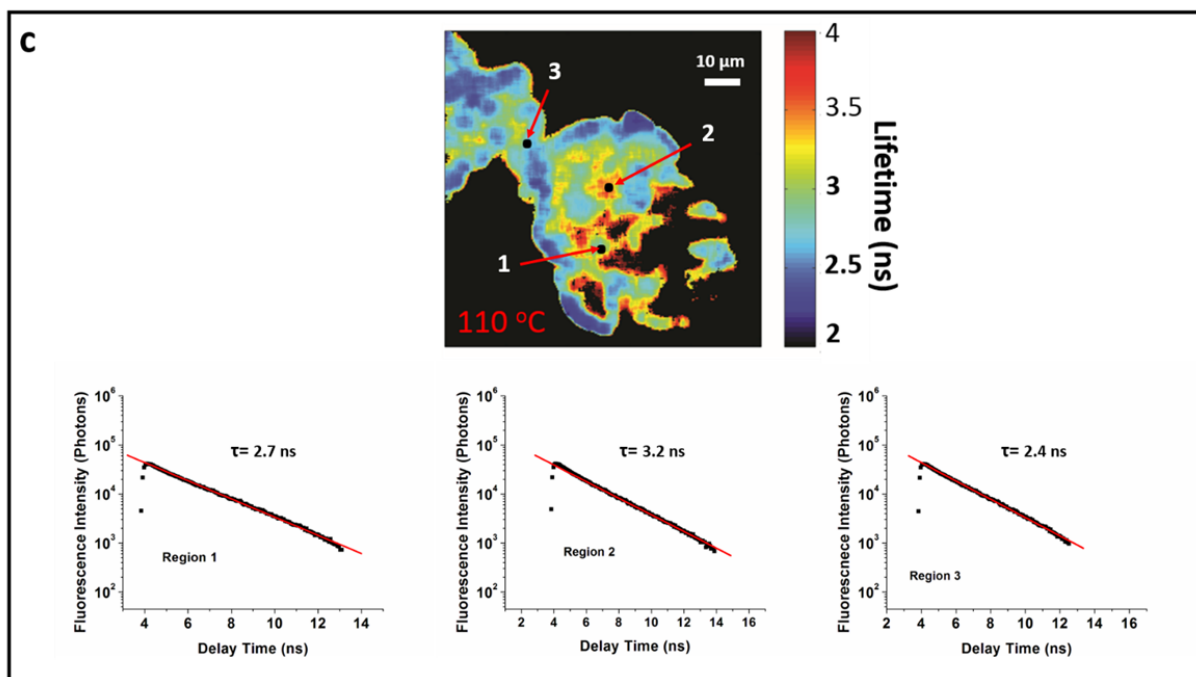
freedom. MP does not have these substituents, which results in greater degrees of freedom resulting in a lower lifetime distribution.



S.I. Figure 3 UV activation of the MP functionalized silk fibroin cross sections cured at 80 °C. Ten minutes of UV irradiation in ambient conditions (a) showed minimal to no activation. After equilibrated with a drop of water and UV irradiated for 10 min (b) Activation was observed demonstrating need for water to achieve significant activation.

The spirolactam ring structure can be opened using UV irradiation. However, in the Rhodamine molecule, this leaves a highly unstable intermediate. Without a stabilizing factor, we have observed that the equilibrium lies to the closed form. After irradiation, we observed very little to no activation of the MP molecules in the cross sections (Figure SI 3a). Upon the presence of water, stable activation can be achieved (Figure SI 3b). The exact stoichiometric requirement of water and the mechanism is not clear. We believe it to be a proton transfer from water generating a hydroxyl group that associates with the cationic center of the amines in the xanthene system. This hypothesis also tells to the thermal deactivation or reversal of the ring opening. This reverse process will generate the spirolactam and inactive dye system plus water. Further mechanistic studies are necessary to confirm this mechanistic pathway.



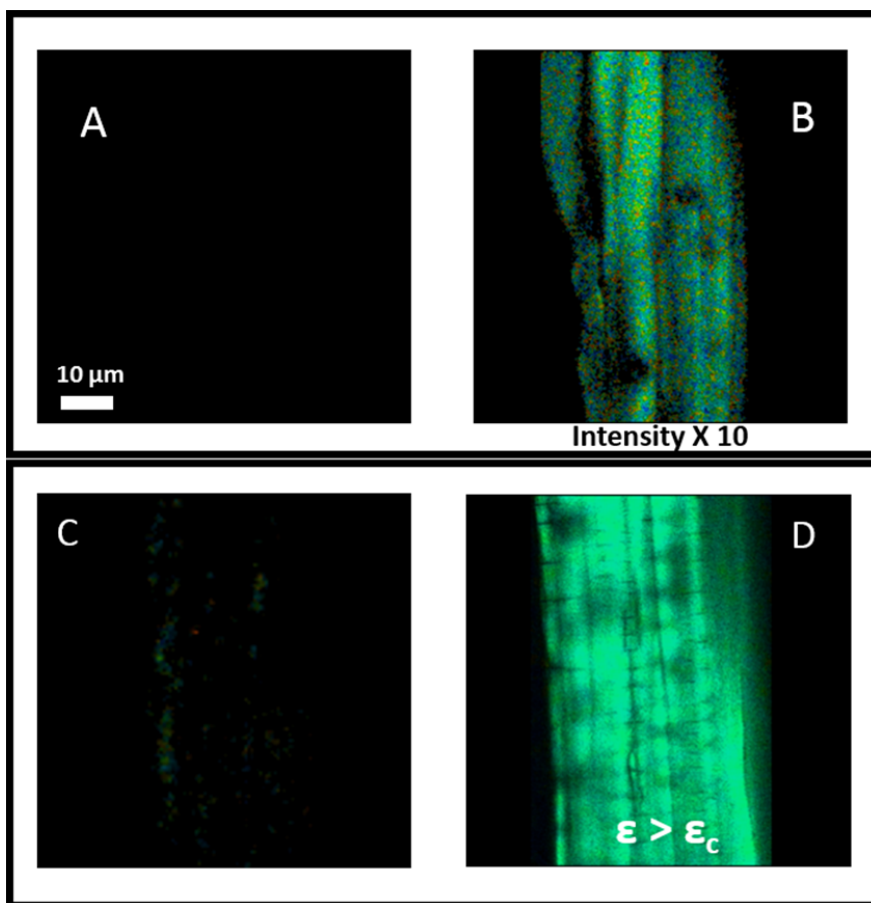


SI Figure 4. Fluorescence decay curves for silk epoxy cross sections. Fluorescence lifetime false color maps of single fiber silk composites with RS reacted at the interface. (a) Composite cured at 23 °C with lifetime decay curves for 3 specific pixels. As seen at 80 °C (b) and 110 °C, the fits to the decay curves are single component exponential. Although the lifetimes may be different, the dye molecules in a given region are similar.

Cross sections of the silk epoxy composites were examined using TP-FLIM to determine extent of reaction between the matrix and the aromatic amines of the MP. The lifetime decay curves were fit with single component exponentials indicating one dye species dominantly present in a given pixel. The shift to longer lifetime is increasingly observed with an increase of cure temperature as can be seen in figure SI-4 panel a-c.

All the fluorescence lifetime curves showed single component fit parameters. Figure SI 4 panel a-c show representative decay curves for the fluorescence lifetime for each cure temperature. This further supports the absence of free dye molecules. However, the single

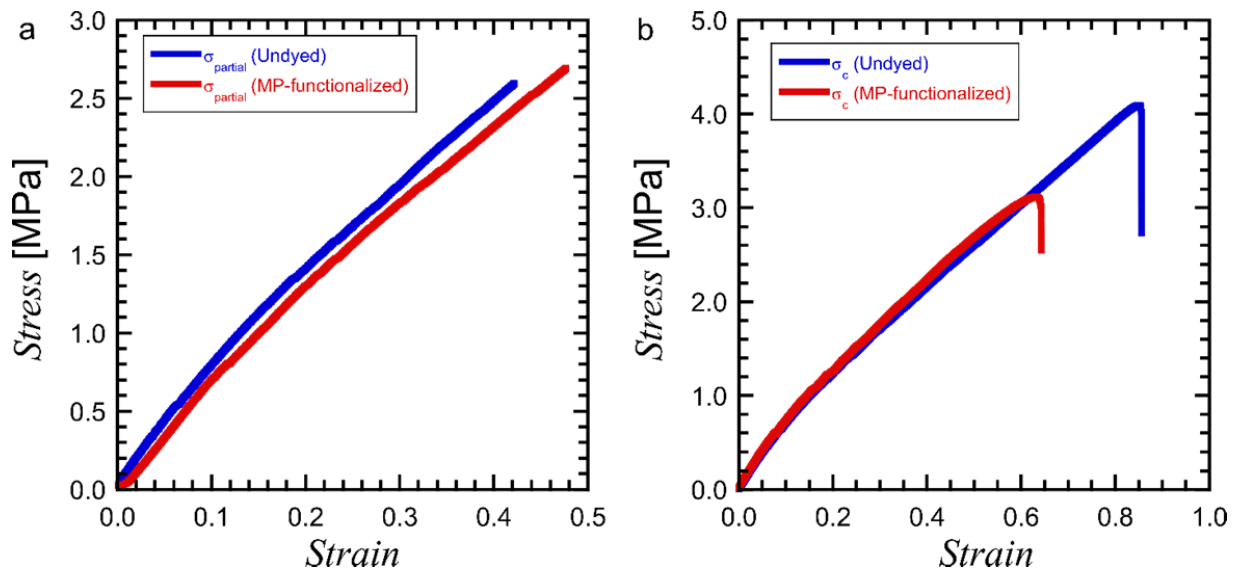
component nature of the curves indicate that the individual regions contain predominately the same extent of reaction or similar dye species. This regioselectivity for chemical reaction of the monomer with the mechanophore is not fully understood. Given silk protein structure, the most likely pathway is the slow disorganization of the crystalline domains allowing for more diffusion of epoxy monomer into the fiber. Given the auto catalytic nature of epoxy resins, this could also be the result of more internalized amorphous alcohol containing regions within the silk macrostructure. Further investigation is needed to determine the exact mechanism behind this process.



S.I. Figure 5. Fluorescence Lifetime images of single fiber composites. Single fiber composites with RS covalently attached to the silk fiber. The CT (top panel) before (A) and after uniaxial strain to sample failure (B) shows no activation within experimental parameters before

applied strain. There is minimal activation at failure, the image intensity is artificially magnified by a factor of 10 to aid the eye. The MP containing composite shows some initial fluorescence prior to applied strain (C). After failure (D), activation is observed throughout the fiber for the MP containing composite above image is at the failure point.

CT fiber composites were fabricated using the same method as the test composites. The samples were stressed by uniaxial deformation until critical failure was reached. Some activation of the CT after failure was observed. The fluorescence was difficult to discern in the image without enhancement. The fluorescence was artificially magnified by a factor of 10 to aid the eye. The lifetime was not calculated for the CT after mechanical activation due to a lack of sufficient photon counts to generate a viable decay curve. The MP showed good activation after critical failure. The image is heterogeneous in character showing dark regions where either debonding did not occur or damage to the fluorescent center itself occurred.



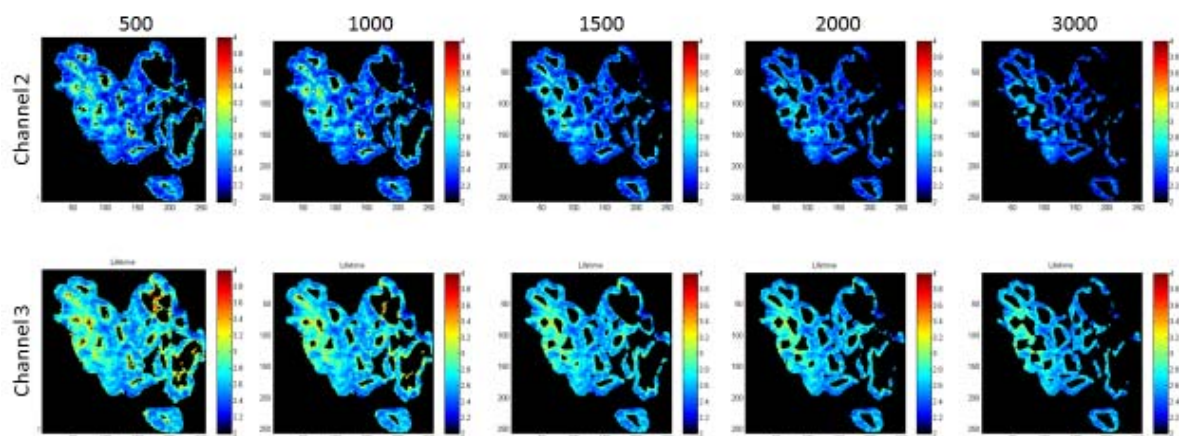
SI Figure 6. The stress-strain behavior of single fiber bundles embedded in epoxy under uniaxial tensile deformation. At approximately (a) $\epsilon=0.4$ and (b) critical strain, the modulus of samples containing fibers with and without MP-functionalization is nearly the same and falls within typical statistical variation. The tensile curves are nearly identical over the entire range

of the test parameters. The failure strain values vary for the two tests shown here. However, this difference of approximately 0.2 is within the normal variation observed for these single fiber bundle tensile experiments.

Silk fibroin fiber bundles were degummed to remove the natural sericin coating. Some fiber bundles were then functionalized with the mechanophore (MP) as described in the experimental section of the main text. Single fiber tensile specimens were then prepared from MP-functionalized and non-functionalized silk fiber bundles by embedding fibers in a degassed, uncured mixture of DGEBA and polyether diamine (polyether copolymer of polypropylene oxide and polyethylene oxide, Jeffamine ED600). Samples were cured in a silicone mold at 80 °C for 18 hours. A dog bone sample geometry was utilized with a gauge length of 14.0 mm and a cross sectional area of 0.8 mm² (0.4 mm by 2.0 mm). Each fiber bundle had a diameter of approximately 0.05 mm. Uniaxial tensile experiments were performed on single fiber samples on an AdMet eXpert 4000 miniature tensile tester. All experiments were conducted at a constant displacement rate of 0.01 mm/s until a desired strain was reached.

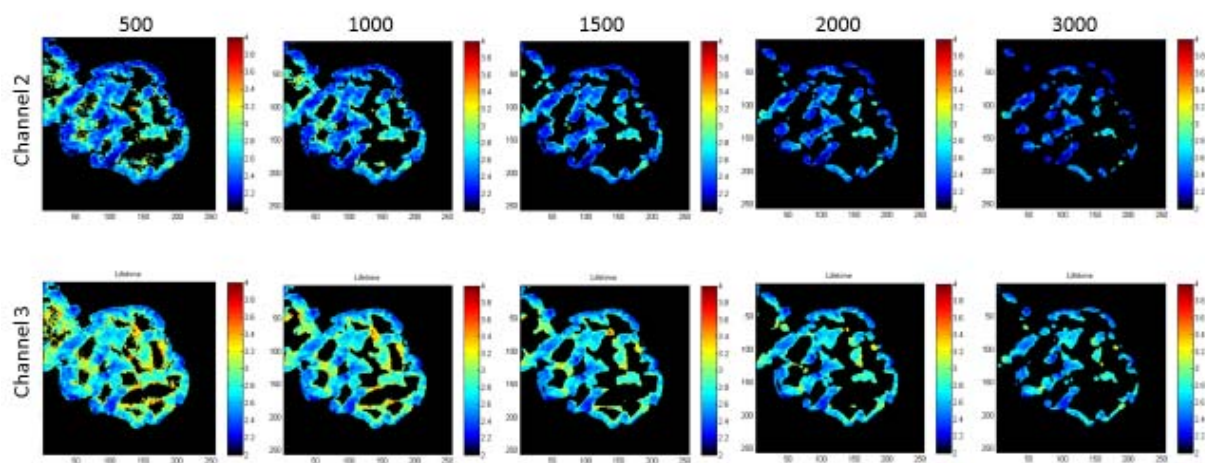
23 °C

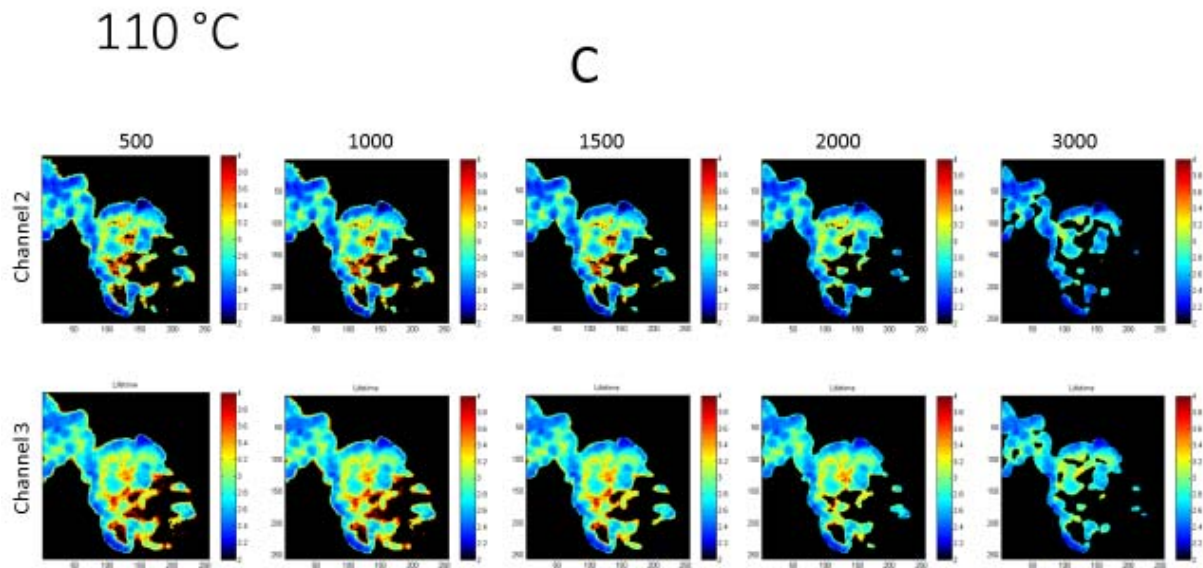
A



80 °C

B

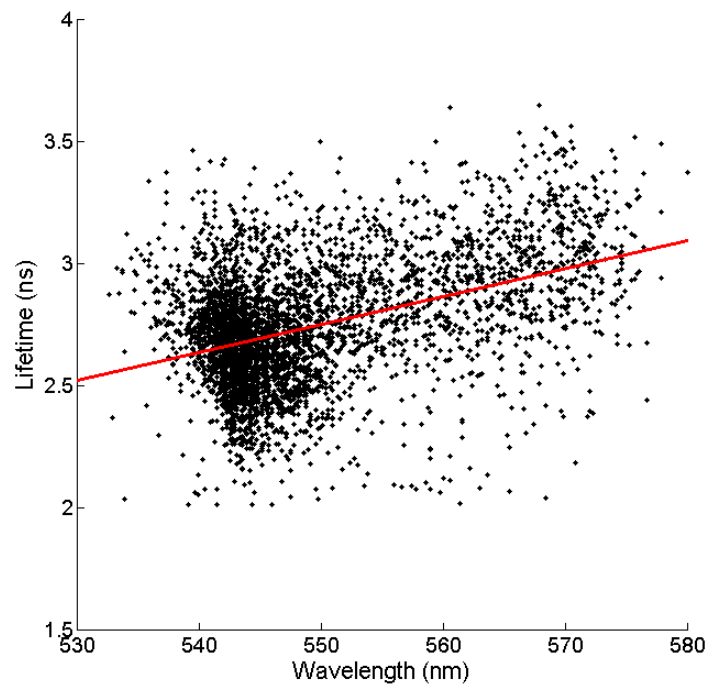




S.I. Figure 7. Lifetime Images thresholding of three cross sections showing qualitative information on dye penetration of the individual fibers. The thresholding values of 500 up to 3000 counts show highest intensity on the periphery of the fiber bundles of (a) 23 °C (b) 80 °C and (c) 110 °C curing temperatures.

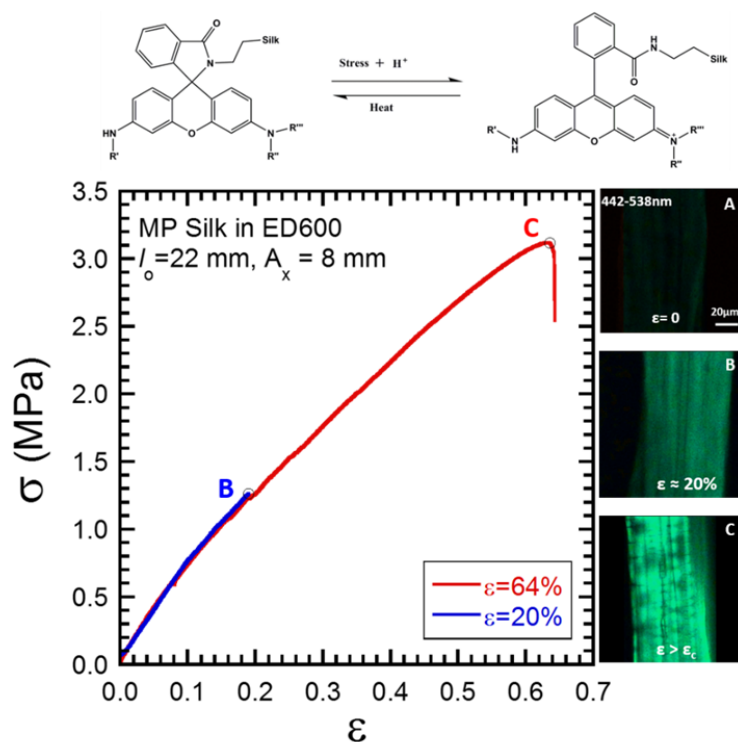
Lifetime and Hyperspectral Fitting

The fluorescence lifetime images were fit with a single exponential where the amplitude and lifetime were fitting parameters. The images were thresholded to avoid fitting pixels with insufficient counts. The resulting lifetimes were subsequently plotted. The hyperspectral images were created by fitting the spectra at each pixel with a log-normal function. The wavelength of the spectral maximum is plotted in the images.



S.I. Figure 8. Correlation between the increase of lifetime and increase in fluorescence emission wavelength for images found in figure 3 b1 and b2. The correlation value obtained was 0.8515 from the red line through the scatter plot.

Table of contents



Polymer composite materials are found throughout the world both natural and artificial in origin. In the vast majority of applications in these arenas, composites serve as structural support or reinforcement. Demand for lightweight tough composites is growing in multiple application spaces such as aerospace, biomaterials, and infrastructure with physical properties as diverse as the applications. The unifying component in all composites is the presence of the interphase. Many measurement techniques and measurement tools have been developed for the study of this crucial region in composite materials. Many of these methods are great for the measurement and study of bulk properties or model systems. However, development of tools that permit the direct observation of interactions at the interphase during applied stress are needed. Here we employ fluorescence lifetime imaging and hyperspectral imaging to

observe activation of a fluorogenic dye at the composite interface as a result of applied stress. The advantages of this system include commercial availability of the dye precursor, and simple one-pot functionalization. The attachment of the dye at the interface is easily monitored through emission wavelength shifts or fluorescence lifetime. Interfacial mechano-responsive dyes have potential for both fundamental studies as well as industrial use as a structural health monitoring tool.